Title: Heterosynaptic interactions between dorsal and ventral hippocampus in individual medium spiny neurons of the nucleus accumbens ventromedial shell

Abbreviated title: Interactions between Hipp inputs in the NAc

Authors: Ashley E. Copenhaver[1], Sydnee Vance[1], Sarah A. Snider[1], Kaela Befano[1], Tara A. LeGates[1,2]

[1] Department of Biological Sciences, University of Maryland, Baltimore County (UMBC)

[2] Department of Physiology and Pharmacology, University of Maryland School of Medicine

Corresponding author:

Tara LeGates, Ph.D.

1000 Hilltop Circle, Interdisciplinary Life Sciences Building 315

Baltimore, MD 21250

tlegates@umbc.edu

Number of pages:

Number of figures: 5 + 1 supplemental figure

Number of words, abstract: 242

Number of words, introduction: 649

Number of words, discussion: 1459

Conflict of interest statement: The authors declare no competing financial interests.

Acknowledgments: We would like to thank Dr. Tagide deCarvalho for her support with microscopy and image analysis, and Dr. Ramesh Chandra for his help with viruses. We would also like to thank Jennifer Pham for her help with injections and Dr. Brian Mathur for his helpful suggestions

on this project. This work was supported by NSF-IOS2402645, T32GM144876-02, T34GM136497, and startup funds provided by UMBC.

ABSTRACT

Establishing learned associations between rewarding stimuli and the context under which those rewards are encountered is critical for survival. Hippocampal input to the nucleus accumbens (NAc) is a key connection involved in integrating environmental information and reward processing to facilitate goal-directed behaviors. This connection consists of two independent pathways originating from the dorsal (dHipp) or ventral (vHipp) hippocampus, which have previously been considered functionally and anatomically distinct. Here, we show overlap in dHipp and vHipp terminal fields in the NAc, which led us to reconsider this view and raise new questions regarding the potential interactions between dHipp and vHipp pathways in the NAc. Using optogenetics, electrophysiology, and transsynaptic labeling in adult male and female mice, we investigated anatomical and functional convergence of dHipp and vHipp in the NAc. We identified a subpopulation of dually innervated cells in the NAc medial shell where dHipp and vHipp inputs are located near one another along dendritic branches. We independently manipulated dHipp and vHipp inputs via two-color optogenetic manipulation during whole-cell electrophysiology recordings to confirm functional dual innervation of individual neurons and revealed heterosynaptic interactions between the two pathways. Altogether, these results demonstrate that dHipp and vHipp dually innervate a subset of neurons in the NAc, suggesting integration of these inputs at the level of individual neurons. Exploring the physiological and behavioral implications of this convergence will offer new insights into how individual neurons incorporate information from distinct inputs and how this integration may shape learning.

SIGNIFICANCE STATEMENT

Forming associations between rewards and the circumstances under which they are experienced is vital for survival. Hipp input to the NAc is essential for associating rewards with their environmental context to effectively guide motivated behaviors. This connection consists of two separate pathways originating from dHipp and vHipp that have long been considered distinct.

Here, we reveal a subpopulation of neurons in the NAc shell innervated by both Hipp subregions as well as heterosynaptic interactions that occur between dHipp and vHipp synapses. These findings suggest that integration of distinct hippocampal information occurs at the single-neuron level, providing a critical mechanism underlying learning and motivated behavior while also opening new avenues for understanding how diverse contextual and reward signals shape decision-making.

INTRODUCTION

The integration of diverse information across neural systems is crucial for driving complex behaviors. The brain dynamically integrates information from multiple sources, enabling organisms to react to stimuli and establish learned associations crucial for survival. Plasticity of and interactions between synapses enables coordinated regulation across multiple inputs, critical for orchestrating cell-wide functional responses (Bailey et al., 2000; Govindarajan et al., 2006; Harvey & Svoboda, 2007; Redondo & Morris, 2011; Schuman & Madison, 1994). However, the mechanisms underlying how convergent inputs interact to shape neuronal responses remain unclear.

The nucleus accumbens (NAc) is a key brain region that integrates diverse information from several brain areas to effectively mediate goal-directed behaviors (Francis & Lobo, 2017; French & Totterdell, 2002; Gruber et al., 2009; Mannella et al., 2013; Marinescu & Labouesse, 2024; Salimpoor et al., 2013; Soares-Cunha et al., 2020). Hippocampal (Hipp) input is a major source of excitatory drive that influences NAc neuron activity (Brog et al., 1993; Calhoon & O'Donnell, 2013; Groenewegen et al., 1987; Kelley & Domesick, 1982; Li et al., 2018; O'Donnell & Grace, 1995; Phillipson & Griffiths, 1985; Trouche et al., 2019), and because of the Hipp's essential role in contextual and spatial learning (Duarte-Guterman et al., 2015; Lamsa & Lau, 2019; Safari et al., 2021; Savage, 2004; Squire, 1992), Hipp-NAc synapses are also key sites for integrating rewards with related contextual and spatial information. Furthermore, the modulation of the

strength of Hipp-NAc synapses is a critical mediator of motivated behaviors and is necessary for supporting contextual- and spatial-based reward learning (Huntley et al., 2020; Ibrahim et al., 2024; Ito et al., 2008, 2008; LeGates et al., 2018; Patterson et al., 2025, p. 202; Pennartz et al., 2011; Sjulson et al., 2018; Trouche et al., 2019; F.-C. Yang & Liang, 2014).

The connection between the Hipp and NAc consists of two independent pathways originating from the dorsal and ventral Hipp (dHipp and vHipp), which are considered functionally and anatomically distinct (Amaral & Witter, 1989; Bannerman et al., 2002; Fanselow & Dong, 2010; Friedman et al., 2002; K. B. Kjelstrup et al., 2008; K. G. Kjelstrup et al., 2002; Roberts et al., 2007; Strange et al., 2014). Notably, the NAc is one of the few regions that receives input from both the dHipp and vHipp (Friedman et al., 2002; Kelley & Domesick, 1982; Phillipson & Griffiths, 1985; Trouche et al., 2019). Although dHipp and vHipp are interconnected within the Hipp (Ishizuka et al., 1990; Swanson & Cowan, 1977; Tao et al., 2021), interactions through connections with other brain regions have been proposed as a mechanism linking cognitive and emotional processes (Fanselow & Dong, 2010). In a multifaceted environment, integration of diverse information is important for properly mediating complex behaviors, and the behavioral complexity governed by these pathways warrants synaptic integration to support learning and memory. These ideas are supported by recent findings demonstrating a key role for convergence of dHipp and vHipp input to the amygdala in observational contextual fear memory (Terranova et al., 2022), yet the synaptic basis of this convergence and whether it is also observed in the NAc remains unknown.

Using a combination of microscopy, electrophysiology, and optogenetics, we identified and characterized a subpopulation of NAc medium spiny neurons (MSNs) that are functionally innervated by both the dHipp and vHipp. dHipp- and vHipp-MSN synapses on these neurons have similar basal synaptic properties, and these synapses are close enough to engage in heterosynaptic interactions likely via presynaptic mechanisms. These findings suggest that convergent Hipp inputs interact at the synaptic level, which may contribute to the integration of spatial and contextual information to modulate motivated behaviors. Overall, understanding the

synaptic integration of dHipp and vHipp inputs in the NAc not only enhances our knowledge of reward-related behaviors, but also offers insight into the fundamental task of neuronal processing and provides a foundation for developing targeted interventions for disorders where these mechanisms are dysregulated.

METHODS

Animals

Male and female C57BL/6J, Drd1a-tdTomato, Ai14, and Ai195 mice were bred in-house. Mice were housed with same-sex cage mates in a temperature- and humidity-controlled environment under a 12:12 light cycle (lights on at 07:00), with food available *ad libitum*. We did not track estrous cycle in females. All experiments were performed in accordance with the regulations set forth by the Institutional Animal Care and Use Committee at the University of Maryland, Baltimore County.

Stereotaxic surgeries

Mice (6-8 weeks old) were anesthetized with 3% isoflurane and underwent stereotaxic surgery. A Hamilton syringe was used to inject adeno-associated viruses (AAV) into the dHipp (in millimeters: from bregma, anterior-posterior (AP), -3.7; medial-lateral (ML), ±2.4; dorsal-ventral (DV), -2.8), vHipp (from bregma, AP, -3.7; ML, ±3.0; DV, -4.8), and NAc (in millimeters: from bregma, anterior-posterior (AP), +1.8; medial-lateral (ML), ±0.6; dorsal-ventral (DV), -4.7). Viruses were injected bilaterally and were infused at a rate of 0.1uL per minute. The injection needle was left in place for 10 minutes following the infusion. After surgery, mice were placed in their home cage on a heating pad for recovery. Carprofen (5mg/kg) was subcutaneously injected daily for 3 days after surgery. Mice recovered for 5-7 weeks for viral expression before anatomical or electrophysiological experiments. Viral constructs pAAV-hSyn-EGFP (Addgene #50465-AAV5) and pAAV-hSyn-mCherry (Addgene #114472-AAV5) were used to visualize dHipp and vHipp

axon terminal fields. Anatomical labeling of dually innervated neurons involved the use of pENN.AAV.hSyn.Cre.WPRE.hGH (AAV1, 1013 titer, UMB Viral Vector Core), pAAV-EF1a-Flpo (AAV1, 1013 titer, UMB Viral Vector Core), and pAAV-hSyn-DIO-EGFP (Addgene #50457-AAV2). Specifically, pENN.AAV.hSyn.Cre.WPRE.hGH and pAAV-EF1a-Flpo were injected into the dHipp or vHipp of Ai195 mice for selective labeling of dually innervated neurons. pENN.AAV.hSyn.Cre.WPRE.hGH and pAAV-EF1a-Flpo were injected into the dHipp or vHipp and pAAV-hSyn-DIO-EGFP was injected in the NAc of Ai14 mice to label neurons single and dually innervated neurons. For optogenetic experiments, viral vectors pAAV-Syn-ChrimsonR-tdT (Addgene ID: 59171-AAV5) and either pAAV-Syn-Chronos-GFP (Addgene ID: 59170-AAV5) or pAAV-hSyn-hChR2(H134R)-EYFP (Addgene ID: 26973-AAV5) were used. For all experiments, injection sites were verified by fluorescence microscopy, and brains with off target expression were removed from the experiment.

Visualization of axon terminal fields and dually innervated neurons

Mice expressing viruses for anatomical tracing experiments were first anesthetized with isoflurane and then perfused with 1X phosphate buffer solution (PBS), followed by 4% paraformaldehyde (PFA). Brains were removed and post-fixed in 4% PFA overnight at 4ºC and were then transferred to 1X PBS and stored at 4ºC for up to 3 weeks. Brains were sectioned (100µm) using a VT1000S Leica Microsystems vibratome. Slices were then mounted with Vectashield Antifade Mounting Medium on slides for imaging.

Images were captured with either a Zeiss LSM 900 Confocal microscope or Zeiss Axio Zoom.V16, both equipped with Zeiss software. To prevent cross talk among channels, images were obtained using sequential scanning to detect multiple fluorophores. To reduce background noise and graininess of images, 2x frame-averaging was used and gain was kept at or below 700. The laser powers used were: EGFP <15% and mCherry or tdTomato <15%. For imaging of

dendritic segments, z-stacks with intervals of 0.2µm were acquired and further analyzed using Imaris.

To quantify individual and dually innervated neurons, images of dorsomedial NAcSh, ventromedial NacSh, ventrolateral NacSh, and ventromedial NAc core were captured on Zeiss LSM 900 Confocal microscope at 40x magnification, equipped with Zeiss software. Images were captured throughout the dorsomedial NAcSh, ventromedial NacSh, ventrolateral NacSh, and ventromedial NAc core. Cells were then manually counted and recounted a day apart. Analysis and counting were done by an experimenter blinded to conditions.

Acute brain slice preparation for electrophysiology

Acute coronal slices containing the nucleus accumbens or hippocampus were prepared for whole-cell patch-clamp electrophysiology. Hipp-containing slices were kept to verify injection sites before proceeding with experiments in the NAc. Animals were deeply anesthetized with isoflurane, decapitated, and brains were quickly dissected and submerged in ice-cold, bubbled (carbogen: 95% O_2/5% CO_2) *N*-methyl-D-glucamine (NMDG) recovery solution containing the following (in mM): 93 NMDG, 2.5 KCl, 1.2 NaH_2PO_4, 11 glucose, 25 $NaHCO_3$, 1.2 $MgCl_2$, and 2.4 $CaCl_2$, pH=7.3-7.4, osmolarity=300-310 mOsm. Using a vibratome (VT1000S, Leica Microsystems), coronal slices (400 µm) were cut in cold, oxygenated NMDG. Slices were transferred to 32-34°C NMDG for 7-12 minutes to recover and were then transferred to room-temperature artificial cerebrospinal fluid (aCSF) containing the following (in mM): 120 NaCl, 3 KCl, 1.0 NaH_2PO_4, 20 glucose, 25 $NaHCO_3$, 1.5 $MgCl_2 \cdot 7H_2O$, and 2.5 $CaCl_2$, pH=7.3-7.4. Slices were allowed to recover for 1-hour at room-temperature before beginning electrophysiological recordings.

Whole-cell recordings

We performed whole-cell patch-clamp recordings using an Axopatch 200B amplifier (Axon Instruments, Molecular Devices) and a Digidata 1550B digitizer (Axon Instruments). Slices were placed in a submersion-type recording chamber and superfused with room-temperature aCSF (flow rate 0.5-1mL/min). Patch pipettes (4-8MΩ) were made from borosilicate glass (World Precision Instruments) using a Sutter Instruments P-97 model puller. Cells were visualized using a 60x water immersion objective (Nikon Eclipse FN-1). All recordings were performed in voltage-clamp conditions from MSNs in the NAc ventromedial shell.

Hipp axon terminals expressing Chrimson, Chronos, or Channelrhodopsin were optogenetically stimulated to record evoked excitatory postsynaptic currents (EPSC). Unless otherwise noted, alternating stimulation was performed every 10s to record EPSCs evoked by either dHipp or vHipp stimulation. For most experiments shown, patch pipettes were filled with a solution containing 130 mM K-gluconate, 5 mM KCl, 2 mM MgCl6-H2O, 10 mM HEPES, 4 mM Mg-ATP, 0.3 mM Na2-GTP, 10 mM Na2-phosphocreatine, and 1 mM EGTA; pH=7.3-7.4; osmolarity=285-295mOsm. High-frequency stimulation of either dHipp or vHipp afferents was performed to induce long-term potentiation of synapses and examine possible long-lasting heterosynaptic plasticity. For experiments determining I-V relationship and AMPA:NMDA receptor ratios, the patch pipette solution was composed of 135 mM CsCl, 2 mM MgCl6-H2O, 10 mM HEPES, 4 mM Mg-ATP, 0.3 mM Na2-GTP, 10 mM Na2-phosphocreatine, 1 mM EGTA, 5 mM QX-314 bromide, and 100 μM spermine; pH=7.3-7.4; osmolarity=285-295mOsm. EPSCs were collected from holding potentials ranging from -80mV to +40mV to create an I-V curve. To calculate AMPA:NMDA receptor ratios, the AMPA component was defined by the peak amplitude at -70mV while the NMDA component was defined by the amplitude at +40mV at 50ms after stimulation. We used the following exclusion criteria to eliminate unhealthy cells and unreliable recordings: 1) We only proceeded with experiments on cells with series resistances <10MΩ, 2)

Cells were excluded if their series resistance changed by >20% (comparing the resistance at the beginning and end of the experiment), 3) Cells in poor health or poor recording status were excluded (i.e. cell partially or fully sealed up, a decrease in holding current >100pA that is consistent with the cell dying, an increase in jitter post HFS, and/or an increase in response failure rate to > 50%).

To minimize the likelihood of cross-contamination between Chrimson and Chronos/ChR2, we conducted control experiments to identify light stimulation intensities that would not cause activation of Chrimson by 470nm light. We found that using light intensities ≤0.5mW prevented cross-contamination (Figure S1), aligning with other published studies (Christoffel et al., 2021; Klapoetke et al., 2014; Xia et al., 2020).

Visualization of dHipp/vHipp terminals with dually innervated neurons

Using a small subset of slices from electrophysiological experiments, dually innervated MSNs were patched and filled with CF633 dye (Biotium). Upon completion of electrophysiology experiments, the 400µm-thick slices were fixed in 4% PFA for 4-8 hours at 4ºC. Slices were then mounted in Invitrogen ProLong Glass Antifade Mountant (Thermo Fisher Scientific, #P36980) on slides with spacers (400µm-thick) for imaging. Images were captured with a Zeiss LSM 900 Confocal microscope equipped with Zeiss software. To prevent cross talk among channels, images were obtained using sequential scanning to detect multiple fluorophores. To reduce background noise and graininess of images, 2x frame-averaging was used and gain was kept at or below 700. The laser powers used were: EGFP <15%, mCherry or tdTomato <15%, CF633 <10%. For imaging of dendritic segments, z-stacks with intervals of 0.2µm were acquired and further analyzed using Imaris.

Quantification, statistical analysis, and reproducibility

We found no statistically significant difference between males and females, so data from male and females are plotted together. Both the number of cells and number of mice is reported for each experiment. Plots represent the mean ± SEM. The sample size (n) per condition represents the number of cells unless otherwise indicated in the figure caption. All statistical analyses were performed using Graphpad Prism 9/10 software. Statistical significance ($p<0.05$) was assessed using parametric or non-parametric versions of paired t tests, or one-way or two-way ANOVA with multiple comparisons. For box plots, the line in the middle of the box is plotted at the median. The box extends from the 25th to 75th percentiles. Whiskers represent minimum and maximum. Figure schematics and experimental timelines were created with BioRender.com.

RESULTS

dHipp and vHipp axon terminal fields overlap in the NAc medial shell

Using viral-mediated labeling to visualize Hipp neurons and their terminal fields, we examined innervation of the NAc by the posterior dHipp and vHipp. We injected an adenoassociated virus (AAV) expressing eYFP into the dHipp and an AAV expressing mCherry into the vHipp (Figure 1a-b). After allowing 5-7 weeks for expression, brains were fixed, sectioned, and imaged using confocal microscopy. We observed dHipp axon terminal fields in the NAc core and lateral shell while the vHipp axon terminal fields were primarily found in the NAc medial shell, in line with previous work (Figure 1c). However, we also observed strong overlap of dHipp and vHipp axon terminal fields in the NAc ventromedial shell (Figure 1c-d), which aligns with the results presented by Brog et al., 1993. 3-D reconstruction of z-stack images of these overlapping axon fields revealed adjacent dHipp and vHipp axons (Figure 1d), highlighting the close proximity of dHipp and vHipp afferents within the ventromedial shell.

Identification of NAc neurons dually innervated by the dHipp and vHipp

Given the apposition of dHipp and vHipp terminals, we sought to determine whether individual neurons were innervated by both hippocampal regions. To do this, we utilized transsynaptic expression of Cre and Flp recombinases to selectively target NAc neurons innervated by dHipp and vHipp pathways (Figure 2a). We injected AAV1-hSyn-Cre into the dHipp and AAV1-Ef1a-Flpo into the vHipp of Ai195 mice in which GcaMP6s is only expressed in the presence of Cre and Flp. This approach allowed for targeted expression of GCaMP6s only in neurons that are innervated by both dHipp and vHipp (Figure 2b). After allowing 5-7 weeks for expression, brains were fixed, sectioned and imaged with confocal microscopy using GCaMP6s to visualize dually innervated neurons. Similar to our observations of terminal field overlap, we observed GCaMP6s-expressing cells in the NAc ventromedial shell (Figure 2c), suggesting dual innervation of NAc neurons by both dHipp and vHipp. Furthermore, examination of GcaMP6s-expressing cells revealed morphology similar to MSNs (Figure 2d), suggesting that primarily NAc MSNs are targeted by both the dHipp and vHipp.

To gain better insight into the proportions of cells innervated by dHipp, vHipp, or both, we used our transsynaptic strategy to differentially label cells innervated by dHipp and vHipp. Specifically, we injected AAV1-hSyn-Cre into the dHipp and AAV1-Ef1a-Flpo into the vHipp of Ai14 mice in which there is Cre-dependent expression of tdTomato. We also injected AAV9-Ef1a-fDIO-eYFP into the NAc of these mice (Figure 2e). As a result, cells innervated by dHipp express tdTomato, cells innervated by vHipp express eYFP, and those innervated by both will express both reporters (Figure 3f-g). Quantification of cells in medial shell revealed approximately 13% of cells were dually innervated. The remainder of cells were innervated by one Hipp subregion (singly innervated). Of these, 26% cells were innervated by dHipp, 61% were innervated by vHipp (Figure 3h).

To determine whether our anatomical results translated into functional convergence, we explored whether MSNs in the NAc ventromedial shell were functionally innervated by the dHipp

and vHipp (AKA “dually innervated”). We focused on MSNs because they comprise 95% of the NAc neuron population, align with the morphology of cells identified by our anatomical tracing studies (Figure 2), and have been shown to receive functional input from either dHipp or vHipp in separate studies. To independently stimulate dHipp and vHipp inputs, we used a dual wavelength optogenetic strategy involving viral expression of Chronos and Chrimson, which are maximally sensitive to different wavelengths of light (480nm and 660nm, respectively) (Klapoetke et al., 2014). AAV2-Syn-Chronos-eYFP or AAV2-Syn-Chrimson-mCherry were injected into the dHipp or vHipp. At least 5 weeks after surgery, coronal brain slices containing the NAc were prepared for electrophysiology. Using whole-cell patch-clamp electrophysiology, we recorded from MSNs in the NAc ventromedial shell and used alternating 473 and 635nm light to measure dHipp and vHipp evoked responses in the MSNs. Keeping the light intensity below 1mW prevented cross-contamination, allowing us to measure and independently manipulate dHipp and vHipp inputs with 473 and 635nm light (Figure S1 and 3a). Using this strategy, we identified a subpopulation of MSNs in the ventromedial shell that responded to both dHipp and vHipp stimulation, demonstrating dual functional innervation of individual NAc MSNs by both dHipp and vHipp (Figure 3a).

Synaptic properties and strengths influence how a neuron responds to and integrates information from distinct inputs, leading us to examine and compare the synaptic profiles of dHipp-MSN and vHipp-MSN synapses in dually innervated neurons. To examine excitatory synaptic strength, we measured AMPAR:NMDAR ratios at dHipp-MSN and vHipp-MSN synapses and found no difference, suggesting that the strength of dHipp- and vHipp-MSN synapses is similar (Figure 3b). We then stimulated each pathway with paired pulses, alternating stimulation such that each pathway was stimulated every 20s. Calculation of paired-pulse ratios (PPR) revealed a significantly greater PPR at vHipp-MSN synapses as compared to dHipp-MSN synapses (Figure 3c), suggesting potential differences in release probability, though this may be driven by a subpopulation of recorded neurons.

Calcium-permeable AMPA receptors (CP-AMPAR) have been identified at ventral subiculum-NAc synapses (Boxer et al., 2023) and have been implicated in NAc plasticity and related behaviors (Carr, 2020; Mameli et al., 2009; McCutcheon et al., 2011; Wolf & Tseng, 2012). Given their role in plasticity and behavior, we examined whether CP-AMPARs were present at dHipp- or vHipp-MSN synapses. Using their characteristic inward rectification and non-linear current-voltage relationship (Cull-Candy et al., 2006; Liu & Zukin, 2007), we performed electrophysiological experiments to identify the predominant population of AMPARs at dHipp and vHipp-MSN synapses. Our results revealed that neither type of synapse contained a significant population of CP-AMPARs (Figure 3d). Altogether, these results indicate that dHipp and vHipp synapses in dually innervated NAc MSNs have similar basal synaptic properties.

We then evaluated the potential for synaptic or dendritic-level interactions between dHipp and vHipp synapses by comparing rise times and the spatial locations of putative dHipp and vHipp synapses. Our rise time analysis revealed similar rise times of dHipp- and vHipp-evoked responses, suggesting that dHipp-MSN and vHipp-MSN synapses are located a similar distance away from the cell body (Figure 3e). We filled a subset of cells electrophysiologically confirmed to be dually innervated with dye (CF633) (Figure 4a), and slices were fixed and prepared for confocal microscopy. We used confocal microscopy and image analysis to measure the spatial location of potential dHipp and vHipp synapses along the dendrites of a dually innervated MSN using the eYFP co-expressed with Chronos, the mCherry co-expressed with Chrimson, and the CF633. From this analysis, we found several examples of dHipp and vHipp puncta that are spatially close (<2um) along distal dendrites of dually innervated MSNs (Figure 4b). Three-dimensional reconstruction of z-stack images revealed overlap of dHipp axons, vHipp axons, and the MSN dendrite, providing further evidence for dHipp and vHipp synapses being spatially close (Figure 4c). Altogether, these results demonstrate functional innervation of individual MSNs by both dHipp and vHipp, where synapses may be close enough to each other to interact at a synaptic or dendritic level.

Heterosynaptic interactions between dHipp and vHipp synapses in NAc MSNs

Synapses that are sufficiently close (<2um apart) can interact and influence each other's activity (Fu et al., 2012; Harvey & Svoboda, 2007; Murakoshi et al., 2011; Xia et al., 2020; Yuste, 2011). Though activity in dHipp and vHipp is not typically temporally coordinated, learning has been found to increase synchrony between dHipp and vHipp (Biane et al., 2023; Morici et al., 2025). Synchronous activity has been shown to induce plasticity through heterosynaptic interactions between adjacent synapses, raising the question of whether the spatial proximity of dHipp and vHipp synapses facilitates heterosynaptic interactions. To address this, we alternated 473nm and 635nm stimulation for 2 minutes to measure EPSCs evoked from independent stimulation of each Hipp pathway. We then synchronized 473nm and 635nm stimulations for 2 minutes to record an evoked EPSC from the simultaneous stimulation of both dHipp and vHipp inputs (Figure 5a,b). If there are no heterosynaptic interactions occurring, then the EPSC amplitudes from the alternating stimulation should be the linear sum of the EPSC amplitude evoked by simultaneous stimulation. Instead, our data show a supralinear summation of separately measured EPSCs (Figure 5b), indicating that heterosynaptic potentiation occurs between dHipp and vHipp synapses. We conducted the same experiment in cells that were not dually innervated and found no difference between EPSC amplitudes evoked by alternating and synchronous stimulation, demonstrating that this effect is specific to dually innervated neurons and not a nonspecific artifact resulting from cross-contamination (Figure 5c).

To better understand the site of synaptic interaction, we compared the failure rates in a separate experiment using minimal stimulation to evoke pathway-specific responses only 50% of the time so that we could appropriately assess an increase or decrease in failure rate during synchronous stimulation. We measured EPSCs evoked from alternating and synchronous stimulation of dHipp-MSN and vHipp-MSN synapses. We then calculated the theoretical probability of getting a response in both the dHipp- and vHipp-MSN pathways, P_{dual}, if they were

stimulated at the same time. Assuming the pathways are independent/non-interacting, we can calculate this probability as the product of their individual success properties: $P_{dual}^{theoretical} = P_{dHipp-MSN}^{success} \cdot P_{vHipp-MSN}^{success}$. We compared this theoretical probability to the observed success rate of sync responses that were classified as dual-evoked responses, finding a significant difference in the observed and theoretical values (Figure 5d) suggesting presynaptic mechanisms may facilitate heterosynaptic interactions between dHipp- and vHipp-MSN synapses.

DISCUSSION

The experiments in this study identified a subpopulation of neurons within the NAc that are dually innervated by dHipp and vHipp. These neurons are primarily located in the NAc ventromedial shell with morphological characteristics that align with those of MSNs. We found that dHipp-MSN and vHipp-MSN synapses in dually innervated neurons have similar basal synaptic properties including comparable release probabilities, synaptic strength, and expression of calcium-impermeable AMPARs. Examination of EPSCs evoked by individual or synchronous stimulation of dHipp and vHipp revealed supralinear summation of EPSCs, suggesting that the synchronous activation of dHipp and vHipp inputs induces short-term heterosynaptic potentiation of dHipp-MSN and vHipp-MSN synapses likely due to presynaptic mechanisms. Altogether, these results reveal mechanisms of dHipp and vHipp synaptic integration within the NAc medial shell, which may be key to supporting the integration of cognitive and emotional processes needed to effectively mediate goal-directed behaviors.

Innervation of the NAc by dHipp and vHipp

Our viral-mediated axon terminal field labeling strategy revealed overlapping dHipp and vHipp innervation patterns within the NAc ventromedial shell. At first glance, this finding seems to contradict previous reports that have suggested that the dHipp and vHipp preferentially innervate

distinct parts of the NAc. However, these reported innervation patterns appear to depend upon the anterior/posterior coordinate used for Hipp viral injections. Most studies have targeted the posterior vHipp and anterior dHipp, showing vHipp projections in the NAc core and medial shell, with dHipp projections in the NAc core and lateral shell (Groenewegen et al., 1987; Ibrahim et al., 2024; Li et al., 2018; Mulder et al., 1998; Scofield et al., 2016). But when the posterior dHipp was targeted with an anterograde tracer, dHipp axon terminal field expression was observed in the NAc ventromedial shell (Ibrahim et al., 2024). Furthermore, the injection of a retrograde tracer into the NAc ventromedial shell showed that neurons located in the posterior dHipp and vHipp were projecting to this area of the NAc (Groenewegen et al., 1987). Our findings align with the latter two studies, as we injected into the posterior Hipp (A/P: -3.7mm) and found overlapping dHipp and vHipp axon terminal fields and dually innervated neurons primarily in the NAc ventromedial shell.

Using a transsynaptic viral-mediated labeling technique, we were able to visualize a small subpopulation of dually innervated neurons that had morphological characteristics similar to MSNs (Figure 2). Because the viruses used for this technique have low efficiency for transsynaptic transfer (Zingg et al., 2017), and the labeling of a dually innervated neuron requires successful transport of both Cre and Flipase virus payloads, it is likely that this anatomical labeling approach underestimates the number of dually innervated neurons in the NAc. This is supported by our electrophysiology experiments, as within a single slice, we were able to record from a larger number of dually innervated neurons than were indicated from the anatomical tracing study. Optimization of this transsynaptic approach would likely provide a better estimate of the number of dually innervated neurons and could aid in identifying whether interneurons, which are sparsely located in the NAc, can receive dual input from dHipp and vHipp.

dHipp and vHipp synapses have similar properties in dually innervated NAc neurons

We found that dHipp- and vHipp-MSN synapses contain primarily calcium-impermeable AMPARs and have similar excitatory synaptic strengths, as measured by AMPA:NMDA receptor ratios (Figure 3). These similarities suggest that, in basal conditions, both pathways may contribute equally to downstream circuit activity. Since the dHipp and vHipp convey different types of behavioral information, this may mean that Hipp-related contextual and sensory cues are equally capable of influencing motivated behaviors. While these similarities are present at baseline, several studies have highlighted changes that occur to dHipp-MSN and vHipp-MSN synapses in response to hormones, neuromodulators, cocaine, external stress, and experience (Floresco et al., 2001; LeGates et al., 2018; Peleg-Raibstein & Feldon, 2006; R. Yang & J. Mogenson, 1984; Sjulson et al., 2018; Williams et al., 2020).

Synaptic interactions between distinct Hipp inputs

The NAc is widely regarded as a critical integrator of several major excitatory inputs and several studies have examined how convergent inputs interact at the synaptic level within the NAc. These studies have revealed intricate interactions mediated by a combination of presynaptic and postsynaptic mechanisms which influence behavioral output (O'Donnell & Grace, 1995; Xia et al., 2020; F.-C. Yang & Liang, 2014; Yu et al., 2022). Further, vHipp input to the NAc can influence how NAc MSNs respond to other excitatory inputs (Calhoon & O'Donnell, 2013; O'Donnell & Grace, 1995), however it is unknown whether these vHipp inputs exert similar regulatory control over dHipp inputs to the NAc. Since the dHipp and vHipp are known to convey distinct types of behavioral information which are critical for driving NAc-mediated motivated behaviors (Ibrahim et al., 2024; Ito et al., 2008; LeGates et al., 2018; Muir et al., 2020; Patterson et al., 2025; Sjulson et al., 2018; Sosa et al., 2020; Trouche et al., 2019; Williams et al., 2020; A. K. Yang et al., 2020; F.-C. Yang & Liang, 2014), we were interested in examining whether dHipp and vHipp inputs are regulated at the synaptic level. Our results revealed that dHipp and vHipp

inputs form synaptic connections with individual MSNs within the NAc ventromedial shell, and these synapses rapidly interact with one another to enhance MSN responses to both regions (Figure 5). Interestingly, activity in dHipp and vHipp is not typically temporally coordinated, however increased synchrony between dHipp and vHipp has been associated with learning(Biane et al., 2023; Morici et al., 2025).The rapid response we observed may provide a basis by which distinct information simultaneously conveyed by dHipp and vHipp can strengthen the NAc's response to external stimuli important for establishing and maintaining learned associations.

Implications of integration that occurs at the synaptic level

Because of the Hipp's essential role in contextual and spatial learning across species and the role of the NAc in reward processing (Fanselow, 2000; Nakazawa et al., 2003; Rudy et al., 2002; Squire, 1992; Steele & Morris, 1999), the connection between the Hipp and NAc is crucial for integrating reward with related contextual and spatial information (Britt et al., 2012; Floresco & Phillips, 1999; Humphries & Prescott, 2010; Ito et al., 2008; Lansink et al., 2008, 2009; LeGates et al., 2018; Pennartz et al., 2011; Sjulson et al., 2018). Functional imaging studies in humans have revealed that greater Hipp-NAc connectivity is associated with positive reinforcement learning (Davidow et al., 2016), increased reward seeking in adolescents (Huntley et al., 2020), and greater positive affect in adults (Heller et al., 2020), implicating a strong link between the strength of Hipp-NAc connectivity and reward-related behaviors. Similar findings have been demonstrated in rodent models which examined Hipp-NAc connectivity using in vivo electrophysiology during spatial and contextual-based reward tasks (Sjulson et al., 2018; Sosa et al., 2020; Trouche et al., 2019). The causal relationship between Hipp-NAc connectivity and reward behaviors has been established with lesion and optogenetic studies, demonstrating that Hipp-NAc synapses are required for contextual- and spatial-based reward tasks (Floresco & Phillips, 1999; Ito et al., 2008, p. 200; LeGates et al., 2018; Trouche et al., 2019; Zhou et al., 2019). This includes our previously published work, which demonstrated that the strength of

ventral Hipp-NAc synapses is a critical mediator of reward-related behaviors (LeGates et al., 2018).

While the dHipp and vHipp are interconnected within the hippocampus (Ishizuka et al., 1990; Swanson & Cowan, 1977; Tao et al., 2021), their interactions in other areas of the brain have been proposed as a mechanism linking cognitive and emotional processes (Fanselow & Dong, 2010) and may be crucial to establishing and retrieving memories. This has been demonstrated in the amygdala, where dHipp and vHipp activate and reactive, respectively, a specific ensemble of neurons to support contextual fear memory (Terranova et al., 2022). The NAc serves as another key brain region that receives both dHipp and vHipp input, where we have revealed rapid synaptic interactions that occur between these pathways. Since Hipp input uniquely exerts such a strong influence over NAc neuron activity and information flow, it is likely these interactions encourage integration of distinct information conveyed by the dHipp and vHipp, critically impacting behavioral outputs.

Altogether, the results presented in this paper provide evidence for the integration of dHipp and vHipp information within individual MSNs of the NAc ventromedial shell. The combination of techniques enabling identification of similar synaptic profiles and rapid interactions occurring between dHipp- and vHipp-MSN synapses provides a foundation for similar studies investigating the integration of distinct inputs at the level of individual neurons. Ultimately, these findings advance our understanding of how spatial and contextual information may contribute to reward-related behaviors that are mediated by the NAc shell while also raising further questions as to how each of these distinct pathways are regulated.

References

Amaral, D. G., & Witter, M. P. (1989). The three-dimensional organization of the hippocampal formation: A review of anatomical data. *Neuroscience*, *31*(3), 571–591. https://doi.org/10.1016/0306-4522(89)90424-7

Bailey, C. H., Giustetto, M., Huang, Y. Y., Hawkins, R. D., & Kandel, E. R. (2000). Is heterosynaptic modulation essential for stabilizing Hebbian plasticity and memory? *Nature Reviews. Neuroscience*, *1*(1), 11–20. https://doi.org/10.1038/35036191

Bannerman, D. M., Deacon, R. M. J., Offen, S., Friswell, J., Grubb, M., & Rawlins, J. N. P. (2002). Double dissociation of function within the hippocampus: Spatial memory and hyponeophagia. *Behavioral Neuroscience*, *116*(5), 884–901. https://doi.org/10.1037/0735-7044.116.5.884

Biane, J. S., Ladow, M. A., Stefanini, F., Boddu, S. P., Fan, A., Hassan, S., Dundar, N., Apodaca-Montano, D. L., Zhou, L. Z., Fayner, V., Woods, N. I., & Kheirbek, M. A. (2023). Neural dynamics underlying associative learning in the dorsal and ventral hippocampus. *Nature Neuroscience*, *26*(5), 798–809. https://doi.org/10.1038/s41593-023-01296-6

Boxer, E. E., Kim, J., Dunn, B., & Aoto, J. (2023). Ventral Subiculum Inputs to Nucleus Accumbens Medial Shell Preferentially Innervate D2R Medium Spiny Neurons and Contain Calcium Permeable AMPARs. *The Journal of Neuroscience*, *43*(7), 1166–1177. https://doi.org/10.1523/JNEUROSCI.1907-22.2022

Britt, J. P., Benaliouad, F., McDevitt, R. A., Stuber, G. D., Wise, R. A., & Bonci, A. (2012). Synaptic and Behavioral Profile of Multiple Glutamatergic Inputs to the Nucleus Accumbens. *Neuron*, *76*(4), 790–803. https://doi.org/10.1016/j.neuron.2012.09.040

Brog, J. S., Salyapongse, A., Deutch, A. Y., & Zahm, D. S. (1993). The patterns of afferent innervation of the core and shell in the “Accumbens” part of the rat ventral striatum: Immunohistochemical detection of retrogradely transported fluoro-gold. *Journal of Comparative Neurology*, *338*(2), 255–278. https://doi.org/10.1002/cne.903380209

Calhoon, G. G., & O'Donnell, P. (2013). Closing the Gate in the Limbic Striatum: Prefrontal Suppression of Hippocampal and Thalamic Inputs. *Neuron*, *78*(1), 181–190. https://doi.org/10.1016/j.neuron.2013.01.032

Carr, K. D. (2020). Homeostatic regulation of reward via synaptic insertion of calcium-permeable AMPA receptors in nucleus accumbens. *Physiology & Behavior*, *219*, 112850. https://doi.org/10.1016/j.physbeh.2020.112850

Christoffel, D. J., Walsh, J. J., Hoerbelt, P., Heifets, B. D., Llorach, P., Lopez, R. C., Ramakrishnan, C., Deisseroth, K., & Malenka, R. C. (2021). Selective filtering of excitatory inputs to nucleus accumbens by dopamine and serotonin. *Proceedings of the National Academy of Sciences*, *118*(24), e2106648118. https://doi.org/10.1073/pnas.2106648118

Cull-Candy, S., Kelly, L., & Farrant, M. (2006). Regulation of Ca2+-permeable AMPA receptors: Synaptic plasticity and beyond. *Current Opinion in Neurobiology*, *16*(3), 288–297. https://doi.org/10.1016/j.conb.2006.05.012

Davidow, J. Y., Foerde, K., Galván, A., & Shohamy, D. (2016). An Upside to Reward Sensitivity: The Hippocampus Supports Enhanced Reinforcement Learning in Adolescence. *Neuron*, *92*(1), 93–99. https://doi.org/10.1016/j.neuron.2016.08.031

Duarte-Guterman, P., Yagi, S., Chow, C., & Galea, L. A. M. (2015). Hippocampal learning, memory, and neurogenesis: Effects of sex and estrogens across the lifespan in adults. *Hormones and Behavior*, *74*, 37–52. https://doi.org/10.1016/j.yhbeh.2015.05.024

Fanselow, M. S. (2000). Contextual fear, gestalt memories, and the hippocampus. *Behavioural Brain Research*, *110*(1–2), 73–81. https://doi.org/10.1016/S0166-4328(99)00186-2

Fanselow, M. S., & Dong, H.-W. (2010). Are The Dorsal and Ventral Hippocampus functionally distinct structures? *Neuron*, *65*(1), 7. https://doi.org/10.1016/j.neuron.2009.11.031

Floresco, S. B., Blaha, C. D., Yang, C. R., & Phillips, A. G. (2001). Modulation of Hippocampal and Amygdalar-Evoked Activity of Nucleus Accumbens Neurons by Dopamine: Cellular

Mechanisms of Input Selection. *The Journal of Neuroscience*, *21*(8), 2851–2860. https://doi.org/10.1523/JNEUROSCI.21-08-02851.2001

Floresco, S. B., & Phillips, A. G. (1999). Dopamine and hippocampal input to the nucleus accumbens play an essential role in the search for food in an unpredictable environment. *Psychobiology*, *27*(2), 277–286. https://doi.org/10.3758/BF03332121

Francis, T. C., & Lobo, M. K. (2017). Emerging Role for Nucleus Accumbens Medium Spiny Neuron Subtypes in Depression. *Biological Psychiatry*, *81*(8), 645–653. https://doi.org/10.1016/j.biopsych.2016.09.007

French, S. J., & Totterdell, S. (2002). Hippocampal and prefrontal cortical inputs monosynaptically converge with individual projection neurons of the nucleus accumbens. *The Journal of Comparative Neurology*, *446*(2), 151–165. https://doi.org/10.1002/cne.10191

Friedman, D. P., Aggleton, J. P., & Saunders, R. C. (2002). Comparison of hippocampal, amygdala, and perirhinal projections to the nucleus accumbens: Combined anterograde and retrograde tracing study in the Macaque brain. *Journal of Comparative Neurology*, *450*(4), 345–365. https://doi.org/10.1002/cne.10336

Fu, M., Yu, X., Lu, J., & Zuo, Y. (2012). Repetitive motor learning induces coordinated formation of clustered dendritic spines in vivo. *Nature*, *483*(7387), 92–95. https://doi.org/10.1038/nature10844

Govindarajan, A., Kelleher, R. J., & Tonegawa, S. (2006). A clustered plasticity model of long-term memory engrams. *Nature Reviews. Neuroscience*, *7*(7), 575–583. https://doi.org/10.1038/nrn1937

Groenewegen, H. J., Der Zee, E. V.-V., Te Kortschot, A., & Witter, M. P. (1987). Organization of the projections from the subiculum to the ventral striatum in the rat. A study using anterograde transport of Phaseolus vulgaris leucoagglutinin. *Neuroscience*, *23*(1), 103–120. https://doi.org/10.1016/0306-4522(87)90275-2

Gruber, A. J., Hussain, R. J., & O'Donnell, P. (2009). The Nucleus Accumbens: A Switchboard for Goal-Directed Behaviors. *PLoS ONE*, *4*(4), e5062. https://doi.org/10.1371/journal.pone.0005062

Harvey, C. D., & Svoboda, K. (2007). Locally dynamic synaptic learning rules in pyramidal neuron dendrites. *Nature*, *450*(7173), 1195–1200. https://doi.org/10.1038/nature06416

Heller, A. S., Shi, T. C., Ezie, C. E. C., Reneau, T. R., Baez, L. M., Gibbons, C. J., & Hartley, C. A. (2020). Association between real-world experiential diversity and positive affect relates to hippocampal–striatal functional connectivity. *Nature Neuroscience*, *23*(7), 800–804. https://doi.org/10.1038/s41593-020-0636-4

Humphries, M. D., & Prescott, T. J. (2010). The ventral basal ganglia, a selection mechanism at the crossroads of space, strategy, and reward. *Progress in Neurobiology*, *90*(4), 385–417. https://doi.org/10.1016/j.pneurobio.2009.11.003

Huntley, E. D., Marusak, H. A., Berman, S. E., Zundel, C. G., Hatfield, J. R. B., Keating, D. P., & Rabinak, C. A. (2020). Adolescent substance use and functional connectivity between the ventral striatum and hippocampus. *Behavioural Brain Research*, *390*, 112678. https://doi.org/10.1016/j.bbr.2020.112678

Ibrahim, K. M., Massaly, N., Yoon, H.-J., Sandoval, R., Widman, A. J., Heuermann, R. J., Williams, S., Post, W., Pathiranage, S., Lintz, T., Zec, A., Park, A., Yu, W., Kash, T. L., Gereau, R. W., & Morón, J. A. (2024). Dorsal hippocampus to nucleus accumbens projections drive reinforcement via activation of accumbal dynorphin neurons. *Nature Communications*, *15*(1), 750. https://doi.org/10.1038/s41467-024-44836-9

Ishizuka, N., Weber, J., & Amaral, D. G. (1990). Organization of intrahippocampal projections originating from CA3 pyramidal cells in the rat. *Journal of Comparative Neurology*, *295*(4), 580–623. https://doi.org/10.1002/cne.902950407

Ito, R., Robbins, T. W., Pennartz, C. M., & Everitt, B. J. (2008). Functional Interaction between the Hippocampus and Nucleus Accumbens Shell Is Necessary for the Acquisition of

Appetitive Spatial Context Conditioning. *Journal of Neuroscience*, *28*(27), 6950–6959. https://doi.org/10.1523/JNEUROSCI.1615-08.2008

Kelley, A. E., & Domesick, V. B. (1982). The distribution of the projection from the hippocampal formation to the nucleus accumbens in the rat: An anterograde and retrograde-horseradish peroxidase study. *Neuroscience*, *7*(10), 2321–2335. https://doi.org/10.1016/0306-4522(82)90198-1

Kjelstrup, K. B., Solstad, T., Brun, V. H., Hafting, T., Leutgeb, S., Witter, M. P., Moser, E. I., & Moser, M.-B. (2008). Finite Scale of Spatial Representation in the Hippocampus. *Science*, *321*(5885), 140–143. https://doi.org/10.1126/science.1157086

Kjelstrup, K. G., Tuvnes, F. A., Steffenach, H.-A., Murison, R., Moser, E. I., & Moser, M.-B. (2002). Reduced fear expression after lesions of the ventral hippocampus. *Proceedings of the National Academy of Sciences*, *99*(16), 10825–10830. https://doi.org/10.1073/pnas.152112399

Klapoetke, N. C., Murata, Y., Kim, S. S., Pulver, S. R., Birdsey-Benson, A., Cho, Y. K., Morimoto, T. K., Chuong, A. S., Carpenter, E. J., Tian, Z., Wang, J., Xie, Y., Yan, Z., Zhang, Y., Chow, B. Y., Surek, B., Melkonian, M., Jayaraman, V., Constantine-Paton, M., … Boyden, E. S. (2014). Independent optical excitation of distinct neural populations. *Nature Methods*, *11*(3), 338–346. https://doi.org/10.1038/nmeth.2836

Lamsa, K., & Lau, P. (2019). Long-term plasticity of hippocampal interneurons during in vivo memory processes. *Current Opinion in Neurobiology*, *54*, 20–27. https://doi.org/10.1016/j.conb.2018.08.006

Lansink, C. S., Goltstein, P. M., Lankelma, J. V., Joosten, R. N. J. M. A., McNaughton, B. L., & Pennartz, C. M. A. (2008). Preferential Reactivation of Motivationally Relevant Information in the Ventral Striatum. *Journal of Neuroscience*, *28*(25), 6372–6382. https://doi.org/10.1523/JNEUROSCI.1054-08.2008

Lansink, C. S., Goltstein, P. M., Lankelma, J. V., McNaughton, B. L., & Pennartz, C. M. A. (2009). Hippocampus Leads Ventral Striatum in Replay of Place-Reward Information. *PLoS Biology*, *7*(8), e1000173. https://doi.org/10.1371/journal.pbio.1000173

LeGates, T. A., Kvarta, M. D., Tooley, J. R., Francis, T. C., Lobo, M. K., Creed, M. C., & Thompson, S. M. (2018). Reward behaviour is regulated by the strength of hippocampus–nucleus accumbens synapses. *Nature*, *564*(7735), 258–262. https://doi.org/10.1038/s41586-018-0740-8

Li, Z., Chen, Z., Fan, G., Li, A., Yuan, J., & Xu, T. (2018). Cell-Type-Specific Afferent Innervation of the Nucleus Accumbens Core and Shell. *Frontiers in Neuroanatomy*, *12*, 84. https://doi.org/10.3389/fnana.2018.00084

Liu, S. J., & Zukin, R. S. (2007). Ca2+-permeable AMPA receptors in synaptic plasticity and neuronal death. *Trends in Neurosciences*, *30*(3), 126–134. https://doi.org/10.1016/j.tins.2007.01.006

Mameli, M., Halbout, B., Creton, C., Engblom, D., Parkitna, J. R., Spanagel, R., & Lüscher, C. (2009). Cocaine-evoked synaptic plasticity: Persistence in the VTA triggers adaptations in the NAc. *Nature Neuroscience*, *12*(8), 1036–1041. https://doi.org/10.1038/nn.2367

Mannella, F., Gurney, K., & Baldassarre, G. (2013). The nucleus accumbens as a nexus between values and goals in goal-directed behavior: A review and a new hypothesis. *Frontiers in Behavioral Neuroscience*, *7*. https://doi.org/10.3389/fnbeh.2013.00135

Marinescu, A.-M., & Labouesse, M. A. (2024). The nucleus accumbens shell: A neural hub at the interface of homeostatic and hedonic feeding. *Frontiers in Neuroscience*, *18*, 1437210. https://doi.org/10.3389/fnins.2024.1437210

McCutcheon, J. E., Wang, X., Tseng, K. Y., Wolf, M. E., & Marinelli, M. (2011). Calcium-Permeable AMPA Receptors Are Present in Nucleus Accumbens Synapses after Prolonged Withdrawal from Cocaine Self-Administration But Not Experimenter-

Administered Cocaine. *The Journal of Neuroscience*, *31*(15), 5737–5743. https://doi.org/10.1523/JNEUROSCI.0350-11.2011

Morici, J. F., Paiva-Lima, I., Silva, A., Pronier, É., & Girardeau, G. (2025). *Dorso-ventral hippocampus neural assemblies reactivate during sleep following an aversive experience* (p. 2024.06.13.598918). bioRxiv. https://doi.org/10.1101/2024.06.13.598918

Muir, J., Tse, Y. C., Iyer, E. S., Biris, J., Cvetkovska, V., Lopez, J., & Bagot, R. C. (2020). Ventral Hippocampal Afferents to Nucleus Accumbens Encode Both Latent Vulnerability and Stress-Induced Susceptibility. *Biological Psychiatry*, *88*(11), 843–854. https://doi.org/10.1016/j.biopsych.2020.05.021

Mulder, A. B., Hodenpijl, M. G., & Lopes Da Silva, F. H. (1998). Electrophysiology of the Hippocampal and Amygdaloid Projections to the Nucleus Accumbens of the Rat: Convergence, Segregation, and Interaction of Inputs. *The Journal of Neuroscience*, *18*(13), 5095–5102. https://doi.org/10.1523/JNEUROSCI.18-13-05095.1998

Murakoshi, H., Wang, H., & Yasuda, R. (2011). Local, persistent activation of Rho GTPases during plasticity of single dendritic spines. *Nature*, *472*(7341), 100–104. https://doi.org/10.1038/nature09823

Nakazawa, K., Sun, L. D., Quirk, M. C., Rondi-Reig, L., Wilson, M. A., & Tonegawa, S. (2003). Hippocampal CA3 NMDA Receptors Are Crucial for Memory Acquisition of One-Time Experience. *Neuron*, *38*(2), 305–315. https://doi.org/10.1016/S0896-6273(03)00165-X

O'Donnell, P., & Grace, A. (1995). Synaptic interactions among excitatory afferents to nucleus accumbens neurons: Hippocampal gating of prefrontal cortical input. *The Journal of Neuroscience*, *15*(5), 3622–3639. https://doi.org/10.1523/JNEUROSCI.15-05-03622.1995

Patterson, D., Khan, N., Collins, E. A., Stewart, N. R., Sassaninejad, K., Yeates, D., Lee, A. C. H., & Ito, R. (2025). Ventral hippocampus to nucleus accumbens shell circuit regulates

approach decisions during motivational conflict. *PLOS Biology*, *23*(1), e3002722. https://doi.org/10.1371/journal.pbio.3002722

Paxinos, G., & Franklin, K. B. J. (2019). *Paxinos and Franklin's The mouse brain in stereotaxic coordinates* (Fifth edition). Academic Press, an imprint of Elsevier.

Peleg-Raibstein, D., & Feldon, J. (2006). Effects of dorsal and ventral hippocampal NMDA stimulation on nucleus accumbens core and shell dopamine release. *Neuropharmacology*, *51*(5), 947–957. https://doi.org/10.1016/j.neuropharm.2006.06.002

Pennartz, C. M. A., Ito, R., Verschure, P. F. M. J., Battaglia, F. P., & Robbins, T. W. (2011). The hippocampal–striatal axis in learning, prediction and goal-directed behavior. *Trends in Neurosciences*, *34*(10), 548–559. https://doi.org/10.1016/j.tins.2011.08.001

Phillipson, O. T., & Griffiths, A. C. (1985). The topographic order of inputs to nucleus accumbens in the rat. *Neuroscience*, *16*(2), 275–296. https://doi.org/10.1016/0306-4522(85)90002-8

R. Yang, C., & J. Mogenson, G. (1984). Electrophysiological responses of neurones in the nucleus accumbens to hippocampal stimulation and the attenuation of the excitatory responses by the mesolimbic dopaminergic system. *Brain Research*, *324*(1), 69–84. https://doi.org/10.1016/0006-8993(84)90623-1

Redondo, R. L., & Morris, R. G. M. (2011). Making memories last: The synaptic tagging and capture hypothesis. *Nature Reviews. Neuroscience*, *12*(1), 17–30. https://doi.org/10.1038/nrn2963

Roberts, A. C., Tomic, D. L., Parkinson, C. H., Roeling, T. A., Cutter, D. J., Robbins, T. W., & Everitt, B. J. (2007). Forebrain connectivity of the prefrontal cortex in the marmoset monkey (*Callithrix jacchus*): An anterograde and retrograde tract-tracing study. *Journal of Comparative Neurology*, *502*(1), 86–112. https://doi.org/10.1002/cne.21300

Rudy, J. W., Barrientos, R. M., & O'Reilly, R. C. (2002). Hippocampal formation supports conditioning to memory of a context. *Behavioral Neuroscience*, *116*(4), 530–538. https://doi.org/10.1037/0735-7044.116.4.530

Safari, S., Ahmadi, N., Mohammadkhani, R., Ghahremani, R., Khajvand-Abedeni, M., Shahidi, S., Komaki, A., Salehi, I., & Karimi, S. A. (2021). Sex differences in spatial learning and memory and hippocampal long-term potentiation at perforant pathway-dentate gyrus (PP-DG) synapses in Wistar rats. *Behavioral and Brain Functions*, *17*(1), 9. https://doi.org/10.1186/s12993-021-00184-y

Salimpoor, V. N., Van Den Bosch, I., Kovacevic, N., McIntosh, A. R., Dagher, A., & Zatorre, R. J. (2013). Interactions Between the Nucleus Accumbens and Auditory Cortices Predict Music Reward Value. *Science*, *340*(6129), 216–219. https://doi.org/10.1126/science.1231059

Savage, L. (2004). The effects of hippocampal lesions on learning, memory, and reward expectancies. *Neurobiology of Learning and Memory*, *82*(2), 109–119. https://doi.org/10.1016/j.nlm.2004.05.002

Schuman, E. M., & Madison, D. V. (1994). Locally distributed synaptic potentiation in the hippocampus. *Science (New York, N.Y.)*, *263*(5146), 532–536. https://doi.org/10.1126/science.8290963

Scofield, M. D., Heinsbroek, J. A., Gipson, C. D., Kupchik, Y. M., Spencer, S., Smith, A. C. W., Roberts-Wolfe, D., & Kalivas, P. W. (2016). The Nucleus Accumbens: Mechanisms of Addiction across Drug Classes Reflect the Importance of Glutamate Homeostasis. *Pharmacological Reviews*, *68*(3), 816–871. https://doi.org/10.1124/pr.116.012484

Sjulson, L., Peyrache, A., Cumpelik, A., Cassataro, D., & Buzsáki, G. (2018). Cocaine Place Conditioning Strengthens Location-Specific Hippocampal Coupling to the Nucleus Accumbens. *Neuron*, *98*(5), 926-934.e5. https://doi.org/10.1016/j.neuron.2018.04.015

Soares-Cunha, C., de Vasconcelos, N. A. P., Coimbra, B., Domingues, A. V., Silva, J. M., Loureiro-Campos, E., Gaspar, R., Sotiropoulos, I., Sousa, N., & Rodrigues, A. J. (2020). Nucleus accumbens medium spiny neurons subtypes signal both reward and aversion. *Molecular Psychiatry*, *25*(12), 3241–3255. https://doi.org/10.1038/s41380-019-0484-3

Sosa, M., Joo, H. R., & Frank, L. M. (2020). Dorsal and Ventral Hippocampal Sharp-Wave Ripples Activate Distinct Nucleus Accumbens Networks. *Neuron*, *105*(4), 725-741.e8. https://doi.org/10.1016/j.neuron.2019.11.022

Squire, L. R. (1992). Memory and the hippocampus: A synthesis from findings with rats, monkeys, and humans. *Psychological Review*, *99*(2), 195–231. https://doi.org/10.1037/0033-295X.99.2.195

Steele, R. J., & Morris, R. G. M. (1999). Delay-dependent impairment of a matching-to-place task with chronic and intrahippocampal infusion of the NMDA-antagonist D-AP5. *Hippocampus*, *9*(2), 118–136. https://doi.org/10.1002/(SICI)1098-1063(1999)9:2<118::AID-HIPO4>3.0.CO;2-8

Strange, B. A., Witter, M. P., Lein, E. S., & Moser, E. I. (2014). Functional organization of the hippocampal longitudinal axis. *Nature Reviews Neuroscience*, *15*(10), 655–669. https://doi.org/10.1038/nrn3785

Swanson, L. W., & Cowan, W. M. (1977). An autoradiographic study of the organization of the efferet connections of the hippocampal formation in the rat. *Journal of Comparative Neurology*, *172*(1), 49–84. https://doi.org/10.1002/cne.901720104

Tao, S., Wang, Y., Peng, J., Zhao, Y., He, X., Yu, X., Liu, Q., Jin, S., & Xu, F. (2021). Whole-Brain Mapping the Direct Inputs of Dorsal and Ventral CA1 Projection Neurons. *Frontiers in Neural Circuits*, *15*, 643230. https://doi.org/10.3389/fncir.2021.643230

Terranova, J. I., Yokose, J., Osanai, H., Marks, W. D., Yamamoto, J., Ogawa, S. K., & Kitamura, T. (2022). Hippocampal-amygdala memory circuits govern experience-dependent

observational fear. *Neuron*, *110*(8), 1416-1431.e13. https://doi.org/10.1016/j.neuron.2022.01.019

Trouche, S., Koren, V., Doig, N. M., Ellender, T. J., El-Gaby, M., Lopes-dos-Santos, V., Reeve, H. M., Perestenko, P. V., Garas, F. N., Magill, P. J., Sharott, A., & Dupret, D. (2019). A Hippocampus-Accumbens Tripartite Neuronal Motif Guides Appetitive Memory in Space. *Cell*, *176*(6), 1393-1406.e16. https://doi.org/10.1016/j.cell.2018.12.037

Williams, E. S., Manning, C. E., Eagle, A. L., Swift-Gallant, A., Duque-Wilckens, N., Chinnusamy, S., Moeser, A., Jordan, C., Leinninger, G., & Robison, A. J. (2020). Androgen-Dependent Excitability of Mouse Ventral Hippocampal Afferents to Nucleus Accumbens Underlies Sex-Specific Susceptibility to Stress. *Biological Psychiatry*, *87*(6), 492–501. https://doi.org/10.1016/j.biopsych.2019.08.006

Wolf, M. E., & Tseng, K. Y. (2012). Calcium-permeable AMPA receptors in the VTA and nucleus accumbens after cocaine exposure: When, how, and why? *Frontiers in Molecular Neuroscience*, *5*. https://doi.org/10.3389/fnmol.2012.00072

Xia, S., Yu, J., Huang, X., Sesack, S. R., Huang, Y. H., Schlüter, O. M., Cao, J.-L., & Dong, Y. (2020). Cortical and Thalamic Interaction with Amygdala-to-Accumbens Synapses. *The Journal of Neuroscience*, *40*(37), 7119–7132. https://doi.org/10.1523/JNEUROSCI.1121-20.2020

Yang, A. K., Mendoza, J. A., Lafferty, C. K., Lacroix, F., & Britt, J. P. (2020). Hippocampal Input to the Nucleus Accumbens Shell Enhances Food Palatability. *Biological Psychiatry*, *87*(7), 597–608. https://doi.org/10.1016/j.biopsych.2019.09.007

Yang, F.-C., & Liang, K. C. (2014). Interactions of the dorsal hippocampus, medial prefrontal cortex and nucleus accumbens in formation of fear memory: Difference in inhibitory avoidance learning and contextual fear conditioning. *Neurobiology of Learning and Memory*, *112*, 186–194. https://doi.org/10.1016/j.nlm.2013.07.017

Yu, J., Sesack, S. R., Huang, Y., Schlüter, O. M., Grace, A. A., & Dong, Y. (2022). Contingent Amygdala Inputs Trigger Heterosynaptic LTP at Hippocampus-To-Accumbens Synapses. *The Journal of Neuroscience*, *42*(34), 6581–6592. https://doi.org/10.1523/JNEUROSCI.0838-22.2022

Yuste, R. (2011). Dendritic Spines and Distributed Circuits. *Neuron*, *71*(5), 772–781. https://doi.org/10.1016/j.neuron.2011.07.024

Zhou, Y., Zhu, H., Liu, Z., Chen, X., Su, X., Ma, C., Tian, Z., Huang, B., Yan, E., Liu, X., & Ma, L. (2019). A ventral CA1 to nucleus accumbens core engram circuit mediates conditioned place preference for cocaine. *Nature Neuroscience*, *22*(12), 1986–1999. https://doi.org/10.1038/s41593-019-0524-y

Zingg, B., Chou, X., Zhang, Z., Mesik, L., Liang, F., Tao, H. W., & Zhang, L. I. (2017). AAV-Mediated Anterograde Transsynaptic Tagging: Mapping Corticocollicular Input-Defined Neural Pathways for Defense Behaviors. *Neuron*, *93*(1), 33–47. https://doi.org/10.1016/j.neuron.2016.11.045

FIGURES

Figure 1. Overlapping dHipp and vHipp axon terminal fields in the NAc. a) Viral injection strategy and experimental timeline. b) Injection sites in the hippocampus. Scale bar=500µm. Atlas image from (Paxinos & Franklin, 2019) c) Overlap of dHipp and vHipp axon terminal fields in the NAc. Scale bar=500µm. Atlas image from (Paxinos & Franklin, 2019) d) Close-up image of overlapping dHipp and vHipp axon terminal fields within the NAc ventromedial shell (top). Scale bar=20µm. With 3-dimensional reconstruction of overlapping axon terminals (bottom). Scale bar= 0.5µm

Figure 2. dHipp^{+}/vHipp^{+}-innervated neurons in the NAc ventromedial shell. a) Viral targeting strategy to selectively label dually innervated neurons b) Cartoon representation of singly vs dually innervated neurons. c) Image of NAc shell depicting GCaMP-expressing cells in the NAc ventromedial shell. Scale bar=100µm. Atlas image from (Paxinos & Franklin, 2019) d) Close-up image of GCaMP-expressing cells in the NAc ventromedial shell, where neuron morphology is consistent with medium spiny neurons. Scale bar=100µm. e) Viral targeting strategy and experimental timeline to label cells innervated by dHipp and vHipp. f) Cartoon representation of singly vs dually innervated neurons. g) Image of cells innervated by dHipp (green) and vHipp (magenta). Dually innervated neurons express both reporters and appear white. Arrowheads point out examples of dually innervated neurons. Scale bar = 100µm h) Quantification of cells innervated single and dually innervated neurons in the NAc medial shell across 4 slices.

Figure 3. Individual NAc neurons are functionally innervated by dHipp and vHipp. a) Viral targeting and optogenetic approach. Electrophysiological recording strategy and representative traces from a dually innervated NAc MSN. b) Similar AMPA:NMDA receptor ratios between dHipp- and vHipp-MSN synapses (n=8 cells/4 mice, p=0.1953, Wilcoxon test). Scale bars on representative traces = 40pA/10ms c) Rectification curve reveals linear relationship, indicating a

lack of calcium-permeable AMPA receptors (n=8 cells/4 mice). d) PPRs recorded from dHipp-MSN and vHipp-MSN synapses on dually innervated neurons (n=16 cells/10 mice, *p=0.0394, Paired t-test). e) Rise time was calculated for dHipp- and vHipp-evoked EPSCs, showcasing similar rise times (n=31 cells/12 mice, *p*=0.2877, Wilcoxon test).

Figure 4. Spatial proximity of dHipp and vHipp puncta along distal dendrites of MSN. a) Cartoon depicting optogenetic, electrophysiology, and cell-filling strategy. b) Combined and separated images depicting an MSN filled with CF633 confirmed to have functional dHipp and vHipp synapses, dHipp puncta (green), vHipp puncta (red). c) Three-dimensional reconstruction of an MSN dendritic segment (cyan) with overlapping/merged dHipp (red) and vHipp (green) afferents.

Figure 5. Heterosynaptic potentiation of dHipp-MSN and vHipp-MSN synapses. a) Viral expression, optogenetic, and electrophysiology strategy. b) Recording from dually innervated MSNs, sequential and synchronous stimulation assay reveals non-linear summation of responses (n=16 cells/10 mice, ***p*=0.0027, Wilcoxon test). c) Sequential and synchronous stimulation assay performed in singly innervated MSNs reveals similar responses to a single wavelength of light or both wavelengths of light (n=16 cells/10 mice, *p*=0.4037, Wilcoxon test). d) Theoretical probability of dual success, P_{exp}, compared with observed dual response success, P_{obs}, during sync period (*n*=9 cells/5 mice, **p*=0.0273, Wilcoxon test).

Figure S1. Prevention of cross-contamination when using 470nm light and the optogenetic protein, Chrimson.

a) Mice were injected with only a Chrimson-containing viral construct and slices were taken at least 5 weeks after surgery to perform electrophysiology. b) A response curve was generated by sampling Chrimson-evoked responses using 470nm light, showing minimal responses at a

laser intensity of 0.75mW, and no Chrimson-evoked response at laser intensities ≤0.5mW. EPSC amplitudes were normalized to the maximum EPSC amplitude.

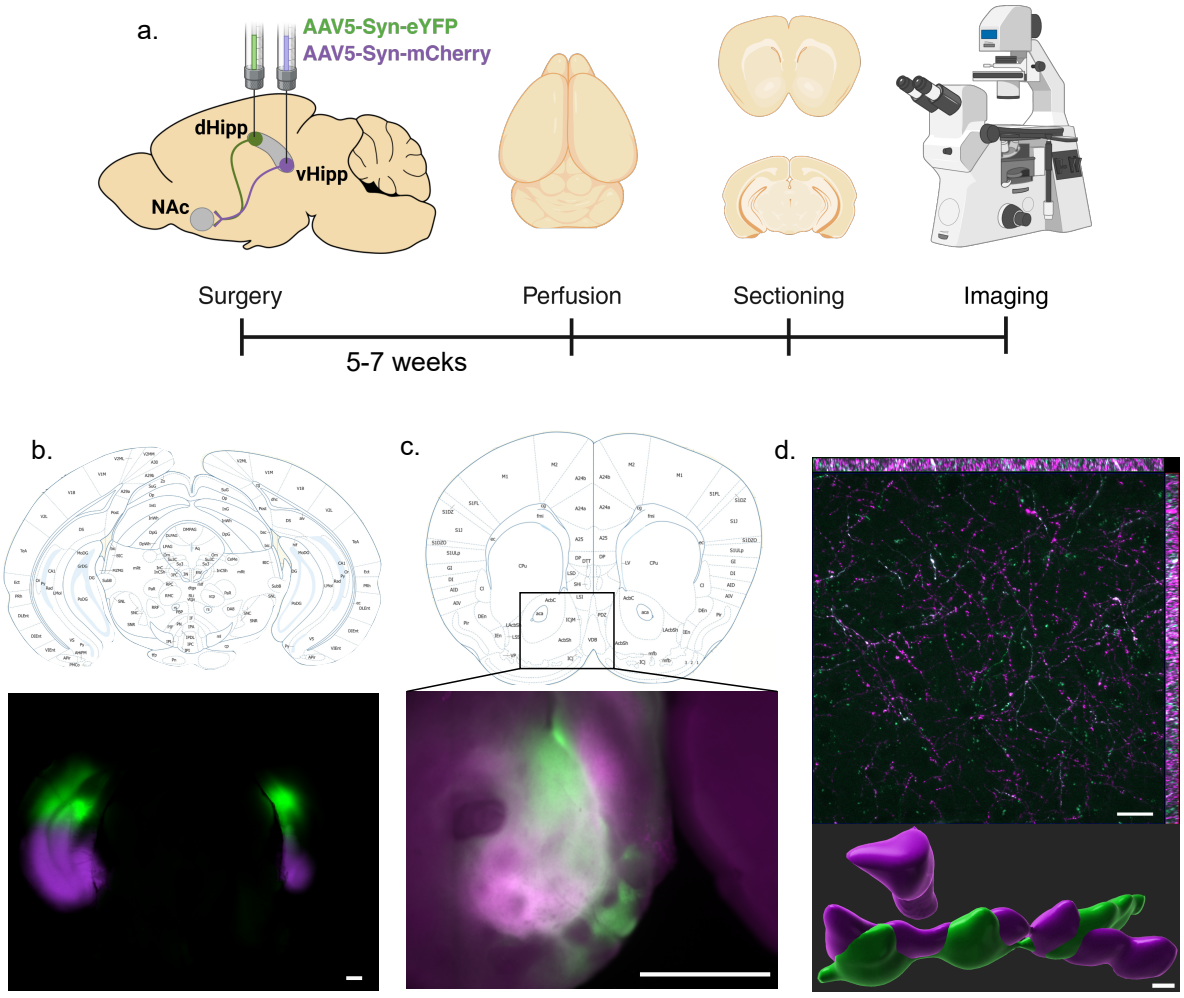
a.
AAV5-Syn-eYFP
AAV5-Syn-mCherry
dHipp
vHipp
NAc
Surgery
Perfusion
Sectioning
Imaging
5-7 weeks
b.
c.
d.

Figure 1

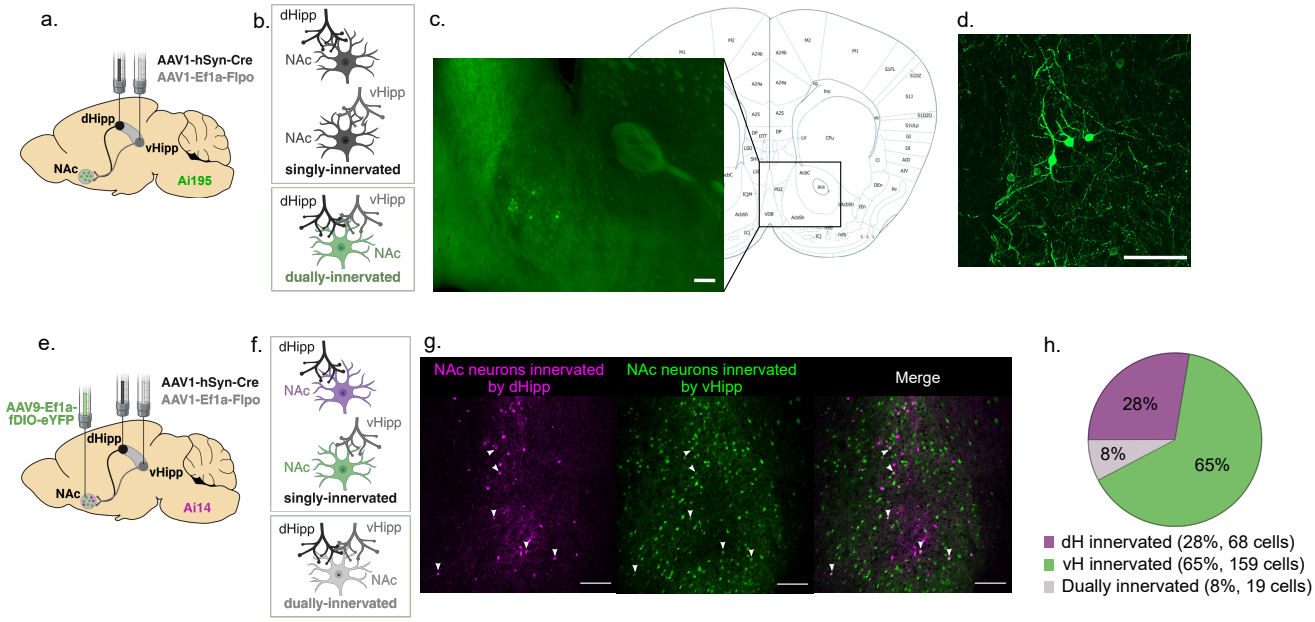
a.
AAV1-hSyn-Cre
AAV1-Ef1a-Flpo
dHipp
vHipp
NAc
Ai195
b.
dHipp
NAc
vHipp
NAc
singly-innervated
dHipp
vHipp
NAc
dually-innervated
c.
d.
e.
AAV9-Ef1a-fDIO-eYFP
AAV1-hSyn-Cre
AAV1-Ef1a-Flpo
dHipp
vHipp
NAc
Ai14
f.
dHipp
NAc
vHipp
NAc
singly-innervated
dHipp
vHipp
NAc
dually-innervated
g.
NAc neurons innervated by dHipp
NAc neurons innervated by vHipp
Merge
h.
28%
8%
65%
dH innervated (28%, 68 cells)
vH innervated (65%, 159 cells)
Dually innervated (8%, 19 cells)

Figure 2

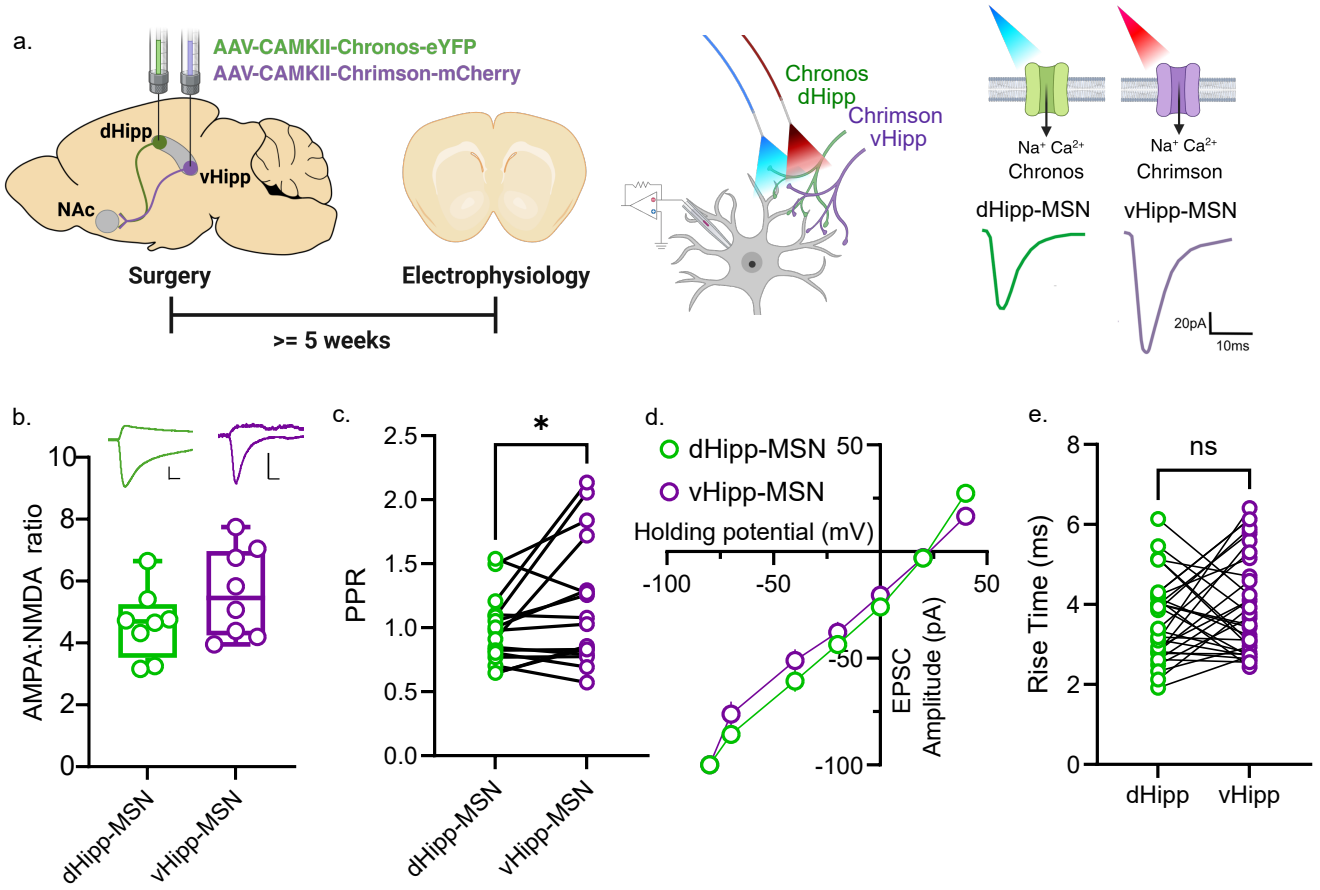
a.
AAV-CAMKII-Chronos-eYFP
AAV-CAMKII-Chrimson-mCherry
dHipp
vHipp
NAc
Surgery
Electrophysiology
>= 5 weeks
Chronos
dHipp
Chrimson
vHipp
Na+ Ca2+
Chronos
Na+ Ca2+
Chrimson
dHipp-MSN
vHipp-MSN
20pA
10ms
b.
AMPA:NMDA ratio
dHipp-MSN
vHipp-MSN
c.
PPR
*
dHipp-MSN
vHipp-MSN
d.
dHipp-MSN
vHipp-MSN
Holding potential (mV)
EPSC Amplitude (pA)
e.
Rise Time (ms)
ns
dHipp
vHipp

Figure 3

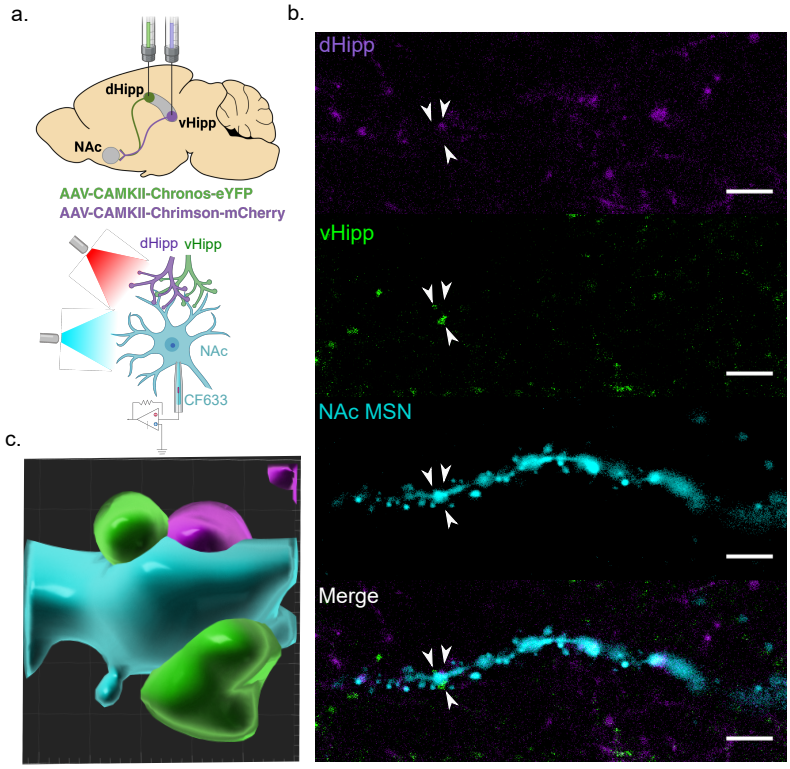
a.
dHipp
vHipp
NAc
AAV-CAMKII-Chronos-eYFP
AAV-CAMKII-Chrimson-mCherry
dHipp vHipp
NAc
CF633
b.
dHipp
vHipp
NAc MSN
Merge
c.

Figure 4

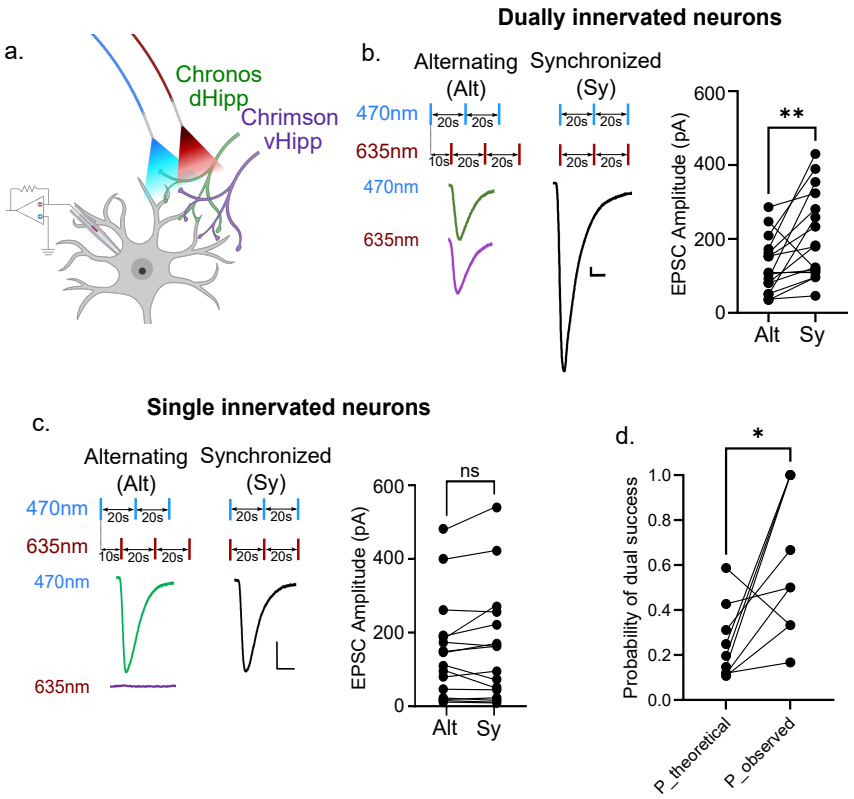
a.
Chronos
dHipp
Chrimson
vHipp
b.
Dually innervated neurons
Alternating
(Alt)
Synchronized
(Sy)
470nm
635nm
20s
10s
EPSC Amplitude (pA)
600
400
200
0
**
Alt
Sy
c.
Single innervated neurons
ns
d.
*
Probability of dual success
1.0
0.8
0.6
0.4
0.2
0.0
P_theoretical
P_observed

Figure 5

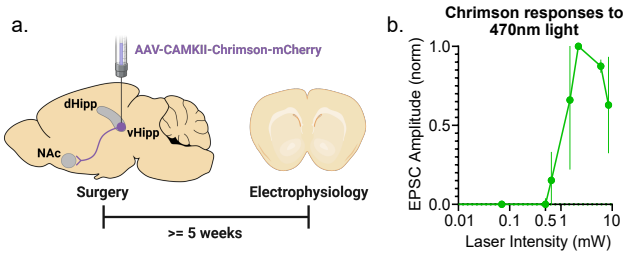

Supplemental Figure 1